TAO, Vol. 9, No. 4, 553-572, December 1998

The Organization of Convection in a Mei-yu Frontal Rainband

Ben Jong-Dao Jou[1] and Shiung-Ming Deng[1]

(Manuscript received 29 October 1997, in final form 5 May 1998)

ABSTRACT

Observations of a convective frontal rainband observed by TAMEX Doppler network were studied in this paper. The results showed that two different types of convection organization were observed in the Mei-yu front. Type A was the shallow convection triggered by cold air surface colliding with the prevailing southwesterly flow. This type of convection was observed on the cold-air leading edge of the surface cold front. The convection was shallow and had the maximum vertical velocity at low levels. The occurrence of maximum rainfall would follow the passage of surface cold front and dissipate rapidly. The appearance of strong vertical wind shear along the interface of the surface cold air and the lifted prevailing southwesterly monsoon flow provided the possibility of forming wave-type disturbances in the post-frontal region through Kelvin-Helmholtz instability. These wave-type disturbances would modulate the convective activity in the post-frontal region. This mechanism resembled a feature very similar to that frequently observed in mid-latitudes: colliding gust fronts associated with thunderstorm outflows.

Type B was the long-lived deep convection systems embedded in the prefrontal rainband region. This type of convection possessed complicated three-dimensional storm-scale features and was produced by a close interaction between the storm-scale features and their immediate mesoscale environmental flows. The tilted updraft, the intense downdraft, the formation of prefrontal mesoscale high pressure systems, and the deflected low-level jet between the frontal zone and the prefrontal mesohigh, all played important roles in triggering, organizing, and maintaining these long-lived convection systems.

(Key words: Frontal rainband, Convection organization, Low-level jet, Scale interaction)

1. INTRODUCTION

Recent observational studies have indicated that precipitation in extratropical cyclones was organized into two-dimensional structures as rainbands. Along the surface cold front, the

[1]Department of Atmospheric Sciences, National Taiwan University, Taipei, Taiwan, ROC

narrow frontal rainband coincided with a line of strong cyclonic shear associated with a low-level jet that laid ahead of and parallel to the surface cold front (Hobbs, 1978). Embedded within these bands were smaller scale regions of intense rainfall called precipitation cores. The cores embedded within the narrow frontal rainbands were ellipsoidal in shape, regularly spaced, and had a definite orientation to the surface cold front. James and Browning (1979) reported that the precipitation cores varied in length from a few kilometers to more than 100 km and had lifetimes of 10 minutes to several hours, and that the cores were oriented slightly clockwise with respect to the synoptic cold front. They also reported that the passage of the narrow frontal rainband was coincident with a windshift at the ground. The shear across the band was about 5×10^{-3} s^{-1}, the width of the shear zone was about 2.5 km and the depth of the convection was about 3 km. Hobbs and Biswas (1979) observed regularly spaced precipitation cores along the narrow frontal rainband. The cores were oriented at an angle of 30° to the front and had a length of 15 km. The cores were also shallow with echo top at about 5 km.

Carbone (1982) reported on the use of a triple Doppler radar network to study a severe frontal rainband in the Central Valley of California. He observed a band of intense precipitation 5 km wide and 250 km long coincident with a zone of strong cyclonic shear. Intense planetary boundary layer forcing of a low-level jet was responsible for producing a two-dimensional prefrontal updraft of 15-20 m s^{-1} with a maximum at 2.1 km above ground level. A vorticity disturbance with a wavelength of 13 km existed in the band. The disturbance organized the precipitation into regularly spaced cores. Carbone suggested that the organization of convection in the narrow frontal rainband was the result of shear instability across it. Hobbs and Persson (1982) observed a strong low-level jet with a maximum speed of 14 m s^{-1} coincident with the narrow frontal rainband. They noted that the circulation in the vicinity of the surface cold front was similar to that observed in laboratory studies of density currents (Simpson, 1969). They suggested that the precipitation cores were the analogues of those unstably stratified regions produced by the overhang of denser fluid over lighter fluid due to frictional retardation at the lower boundary in these currents.

Ross and Orlanski (1982) and Orlanski and Ross (1984) reported a numerical simulation of an observed cold front. The model included an explicit representation of the moist convective processes. In case without moist processes, the frontal zone was characterized by a low-level convergence zone, a two-dimensional line vortex, and a positive potential temperature anomaly. In case with moisture, the frontal feature intensified. The maximum vorticity increased by 70% and the temperature anomaly doubled. Of more interest was the development of cellular convection along the surface front. This suggested that the organization of convection in the vicinity of surface front appeared to be the result of an interaction between the convective activity and the horizontal shear of the background frontal scale flow.

A Mei-yu front passed through the dense observational network of TAMEX (Taiwan Area Mesoscale Experiment) on June 24-25 1987. A convective rainband formed over the frontal surface when the surface front approached Taiwan Strait. Embedded within the band, smaller scale precipitation cores of intense rainfall similar to those observed in mid-latitudes were present. More interestingly, the band-type convection gradually evolved into a multicellular mesoscale convective systems (MCSs) and propagated slowly southward along the west coastal area of Taiwan. This system brought heavy precipitation to northern and central

Taiwan and caused a flooding problem in Taichung area.

This case has been studied quite extensively both by using observational data (Chi and Chen, 1989; Lin *et al.*, 1989; Jou and Deng, 1992; Lin *et al.*, 1992; Lin *et al.*, 1993; Li *et al.*, 1997) and numerical models (Mannouji and Kurihara, 1990; Kuo and Wang, 1995). Chi and Chen (1989) gave a synoptic overview and a satellite survey of the MCS of this case. Lin *et al.* (1989) using dual-Doppler radar data of CAA and CP4 to show that some long-lived convective systems were embedded in the rainband when the system was still in the northern Taiwan Strait and in its early stage. Lin *et al.* (1992 and 1993) used dual-Doppler radar data of CP4 and TOGA to study the kinematic and thermodynamic properties of the rainband system while it was approaching the coastal region of central Taiwan. The results showed that the convective rainband was lifted by the surface cold front and that the rainband was maintained by the interaction between the cold outflows from the previous convective cells and the prevailing low-level southwesterly. In a study of the mesoscale environment, Li *et al.* (1997) pointed out that, as the Mei-yu front advanced southeastward, the post-frontal cold air in the lowest levels was retarded by the hilly terrain along the southeastern China coast. As a result, a low-level wind shift line associated with a pressure trough at the 850hPa level moved over the Taiwan Strait before the arrival of the surface front. The westerly flow behind the trough interacted with the barrier jet, which was caused by the interaction between the prefrontal southwest monsoon flow and the island mountain, to form a low-level convergence zone. The long-lived rainband developed within the low-level convergence zone and moved southeastward with the wind-shift line.

In this paper, we are to present results from single and dual-Doppler analyses of this case from CAA and CP4 radars. In Jou and Deng (1992), the role of low-level jet (LLJ) in triggering and organizing the MCSs along the Mei-yu front had been studied. It was pointed out that the LLJ decelerated when nearing to the major convective precipitation region and showed a distinct diffluent flow feature. This flow feature provides a concentrated warm and moist air convergence near the surface front and is favorable for the continuation of the convection activity. In this paper, we emphasize the organization of convection associated with the frontal rainband. More details of the kinematic and dynamic structures of the convection embedded within the rainband are discussed. In section 2, data used is described and in section 3 a brief overview is given. The shallow convection in the Mei-yu front is described first by using single Doppler data in section 4, and in section 5 the deep convection in the Mei-yu front is described by using the dual-Doppler synthesized wind data and retrieved thermodynamic fields. Finally, a concluding remark is given to summarize the results.

2. DATA AND ANALYSIS PROCEDURE

The data used in this study are taken from the multiple Doppler radar network operated during the TAMEX period. The single Doppler analysis is based on data from CAA Doppler radar. The rectangle shown in Figure 1 indicates the area of dual-Doppler analysis. Fields synthesized from CAA and CP4 radars are analyzed with origin (0,0) at the left bottom corner. The long axis of the rectangle rotates 35° counterclockwise from the east. The analysis domain is 100km x 70km and the grid space is 1 km. The detailed analysis procedures and data used

can be found in Jou and Deng (1992) and will not be repeated here.

3. THE FRONTAL RAINBAND AND ITS ENVIRONMENT

In Figure 1, the radar reflectivity at 1800UTC 24 June 1987 observed by CAA Doppler radar is given. Mesoscale surface analyses showed that the surface front moved southeastward with speed 4 m/s. The rainband moved in the same direction and speed as the surface front. The major convection occurred in a region surrounded by the surface front and island topography with a strong southwesterly LLJ prevailing in between. The convective rainband had a spatial extent of approximately 50 km in width and 200 km in length. The rainband had a multi-cellular structure. New cells formed at the southwestern edge of the front and then propagated eastward. Cells dissipated rapidly when approaching the coastal area. In this study, the

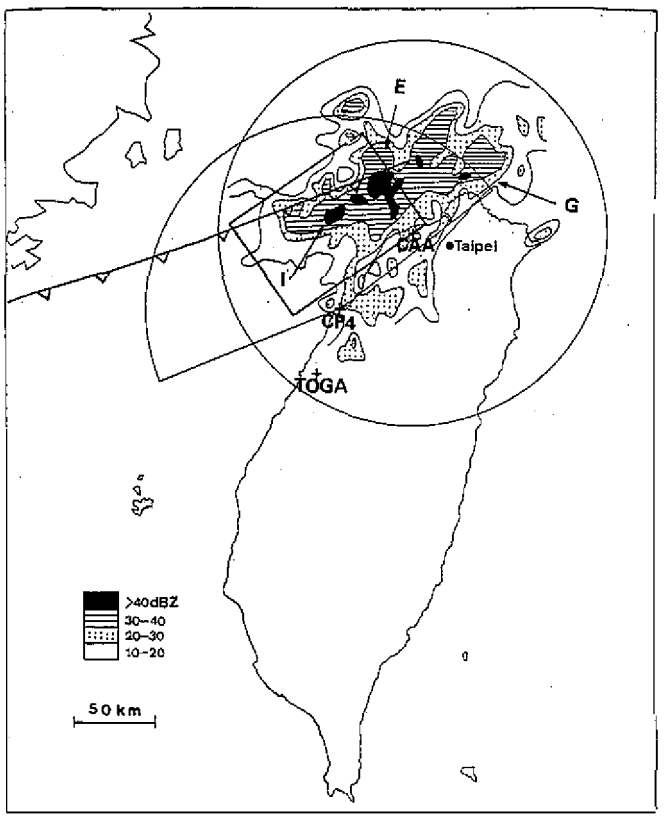

Fig. 1. Doppler radar network for TAMEX. The CAA radar was in a VAD mode and CP4 in sector mode. The small rectangle (100km X 70km) is the area dual-Doppler synthesis was performed. The shaded region shows the reflectivity pattern at 3 km on 1800UTC June 24 1987. The position of the surface front is also indicated.

convective cells were identified by reflectivity patterns taken from CAA Doppler radar from 1430 to 1920UTC 24 June 1987. The criteria for the cell identification are: (1)the existence of closed reflectivity contour of 40 dBZ of radar reflectivity in constant-altitude plan position indicator (CAPPI) maps; (2)the size of the cell must be larger than 10km ×10km; and (3)the cell lifetime must be longer than 30minutes. In Figure 1, cell E, I and G were identified based on those above criteria.

Figure 2 show the holograph of environmental horizontal winds at various heights taken from Panchiao sounding at 1200UTC 24 June. The propagation speed and direction of each individual precipitation cell were also given. Most of cells moved in the direction of the mean environmental wind in the middle troposphere (about 10-15 ms^{-1}) and had a large angle to the direction of rainband movement. Besides this, a few cells moved more slowly than the mean environment wind, as cells E and I in Figure 1. These slower moving cells also possessed longer lifetimes than other cells, *i.e.*, average lifetime for all 15 cells shown in Figure 2 was 100 minutes, and cell E was 4 hours and cell I was 2.5 hours. It was noted that, from vertical

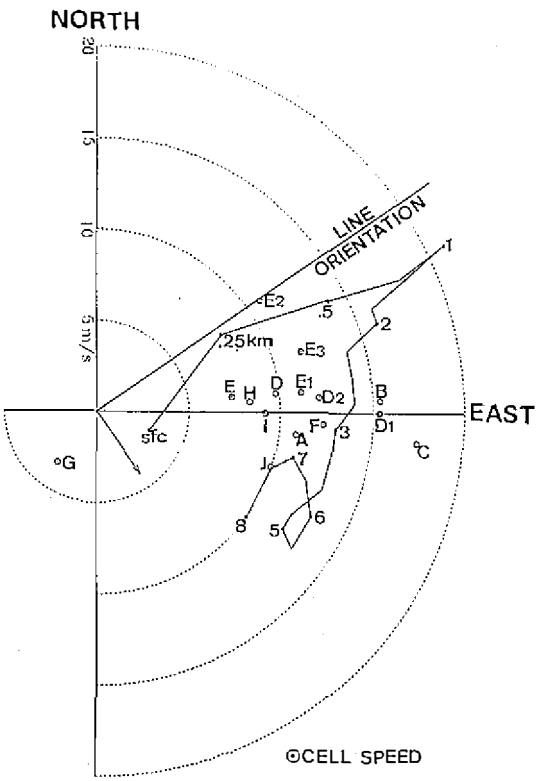

Fig. 2. Hodograph of Panchiao sounding on 1200UTC June 24 1987. Numbers indicate the height in km. The propagation speed and direction of each individual precipitation core identified through reflectivity maps are given (A , B , C , etc).

profiles of reflectivity, cell E and cell I both developed into deep convective systems (30dBZ reflectivity contour line penetrated above 10 km height) and possessed strong precipitation echoes (larger than 45 dBZ) at 2-4 km height. Furthermore, the reflectivity of cell E elongated southeastward in a direction parallel to the environmental shear vector between the lower and middle troposphere. These long-lived convective cells revealed quite complicated three-dimensional storm-scale features, as suggested by dual-Doppler analyses. Detailed results will be presented in section 5.

4. SHALLOW CONVECTIONS IN THE MEI-YU FRONT

It is noted that, within the frontal rainband, one cell moved quite differently from the others, *i.e.*, the G cell. Cell G moved south-southwestward in direction against the low-level environment winds. A further investigation of cell G is given in the following.

Figure 3a shows the 0.5° PPI reflectivity and radial winds taken from CAA Doppler radar on 1800UTC 24 June 1987. A low-level wind-shift line laid 20 km north of the radar. Intense precipitation was present over the cold-air leading edge (northward) of the wind-shift line. The reflectivity intensity dissipated rapidly away from the wind-shift line. Figure 3b showed the mean structure (averaged by 10 beams) of reflectivity and the velocity component parallel to the long axis of rectangle (in NE-SW direction) as depicted in Figure 3a. Most noticeable was the deep southwesterly flow prevailing in the lower and middle troposphere. To the south of the wind-shift line, the maximum SW wind was at 1 km height above sea level (ASL). But, to the north of the wind-shift line, the maximum SW wind was lifted to 2.5 km height ASL and intensified. Flow from the north was less than 1km deep and had maximum intensity (~8 ms^{-1}) near the surface. Intense vertical shear (15-20 $ms^{-1}km^{-1}$) along the upper surface of the cold air was shown. The convection associated with the wind-shift line was rather shallow (below 8 km for 10 dBZ contour line) in spite of strong horizontal convergence present at the wind-shift line. The maximum of reflectivity was at low levels. Reflectivity field revealed wave structure north of the wind-shift line in the middle and lower troposphere. This feature is depicted more clearly in Figure 3c, in which the reflectivity field overlaying the estimated vertical velocity along line A-B is given. The vertical velocity was calculated by assuming two-dimensionality of the flow structure. $4ms^{-1}$ updraft was obtained on top of the cold-air leading edge at height 1.5 km. Away from the leading edge, the intensity of the vertical velocity decreased rapidly. The vertical velocity field revealed pronounced wave structure on top of the cold air and was consistent with the reflectivity pattern.

Strictly speaking, it is probably misleading to state that the convective cell G was moving south-southwestward as marked in Figure 2. According to the cell identification criteria stated earlier, the intense precipitation areas (for those areas with reflectivity intensities larger than 40 dBZ) were traced. The traced trajectory is identified as the cell movement. It should be mentioned that the time resolution of radar reflectivity data was 10 minutes. Based on this data set, it was difficult to identify in detail the life cycle of any individual convective cell. Careful examination of series reflectivity maps in the case of cell G suggested that the strong reflectivity cores were newly developed convective cells initiated at the leading edge of the low-level wind-shift line at a discrete time. The convection was initiated at the leading edge of the cold

air due to colliding between the local surface front and the prevailing southwesterly flows. The convection dissipated rapidly while moving toward cold air. Thus, the true cell motion relative to the wind-shift line for cell G should be northeastward instead of southwestward. The propagation direction and speed of cell G depicted in Figure 2 should be interpreted as the propagation direction and speed of the low-level wind-shift line. This statement is consistent with what was observed at the surface station in the CAA radar site (Figure 3d). Combining the data

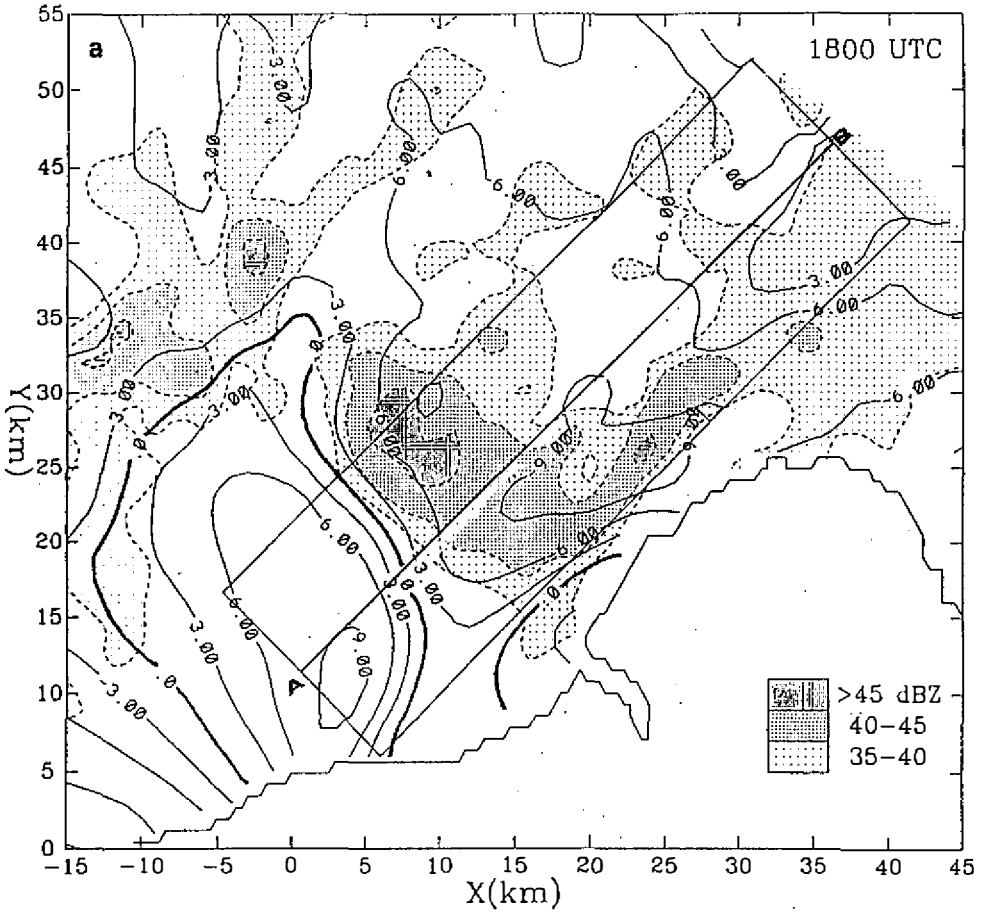

Fig. 3. (a) Reflectivity (dash line) and radial velocity (solid line) at 0.5 PPI of CAA radar on 1800UTC June 24 1987. Positive values represent flow receding from the radar. (b) Mean structure of reflectivity (short dash line) and velocity component parallel to line a-b in (a). (c) Reflectivity field superimposed vertical velocity along line a-b. The bold solid line indicates the wind-shift line. (d) Surface observations taken from CKS International Airport (CAA Doppler radar site) on 25 June (local time). The triangle at the bottom indicates the time of frontal passage.

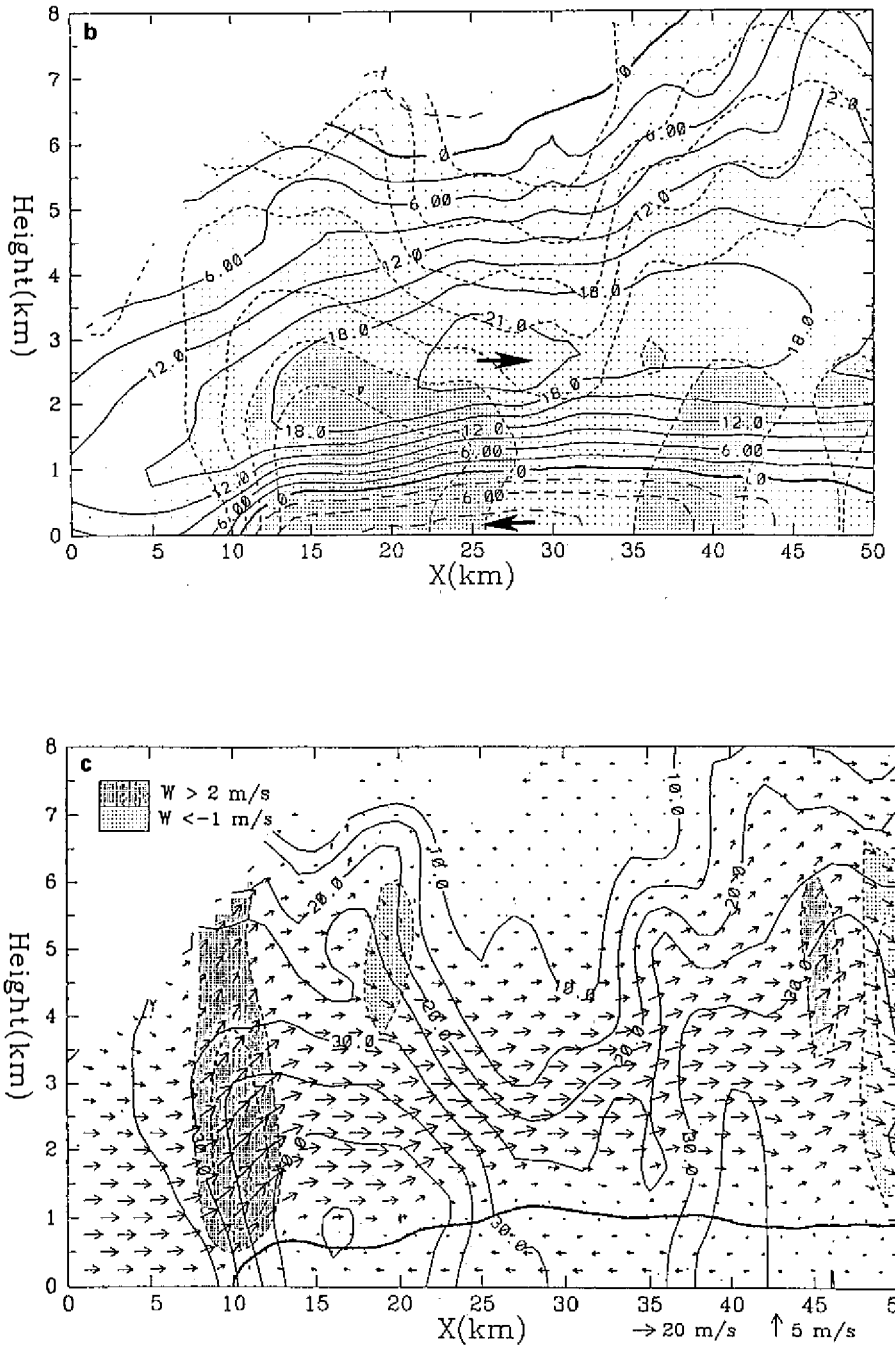

(*Fig. 3.* continued)

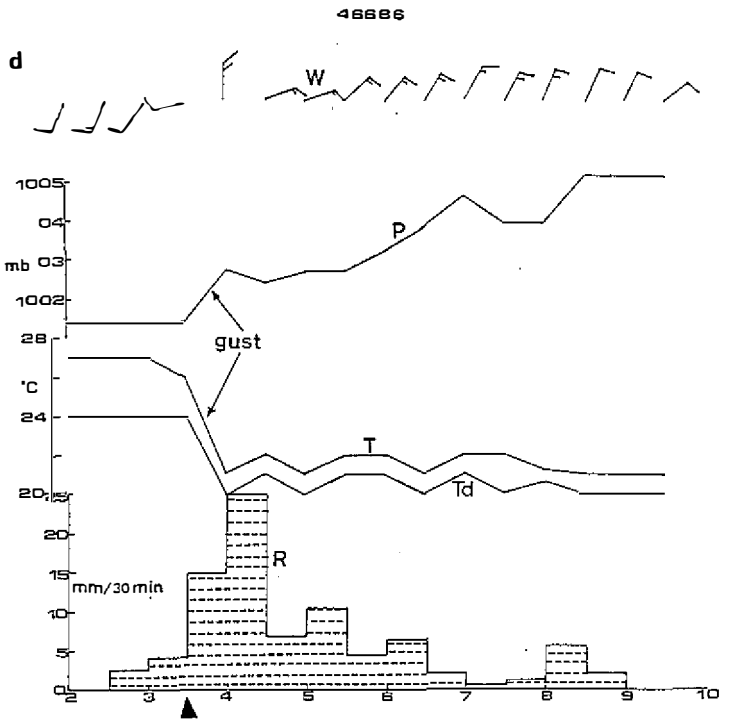

(*Fig. 3.* continued)

shown in Figure 3, we may conclude that the low-level wind-shift line observed by the CAA Doppler radar was the cold-air leading edge of the surface Mei-yu front depicted in Figure 1. The occurrence of shallow convection in Mei-yu front was initiated due to colliding warm southwesterly and cold northerly flows. The mechanism was rather similar to the initiation of convection by colliding gust fronts in thunderstorm outflows (Wakimoto, 1982; Mueller and Carbone, 1987). The presence of shallow convection in the Mei-yu front was also reported in Trier *et al.*(1990).

Wave structure of convection on top of the cold air was possibly caused by Kelvin-Helmholtz instability induced by intense vertical shear on the interface region or internal gravity waves triggered by the convective activity in a stable-stratified atmosphere. In a recent study, Weckwerth and Wakimoto (1992) showed that a combination of Kelvin-Helmholtz and internal gravity wave activity had interacted to produce a favorable locations for initiation and organization of convection atop the thunderstorm cold-air outflows based on MIST data.

5. DEEP CONVECTIONS IN THE MEI-YU FRONT

5.1 Kinematic and Thermodynamic Structure

Figures 4a-c show the dual-Doppler synthesized system-relative horizontal wind field, the reflectivity field, and the horizontal divergence field at 1km height on 1730, 1800, and

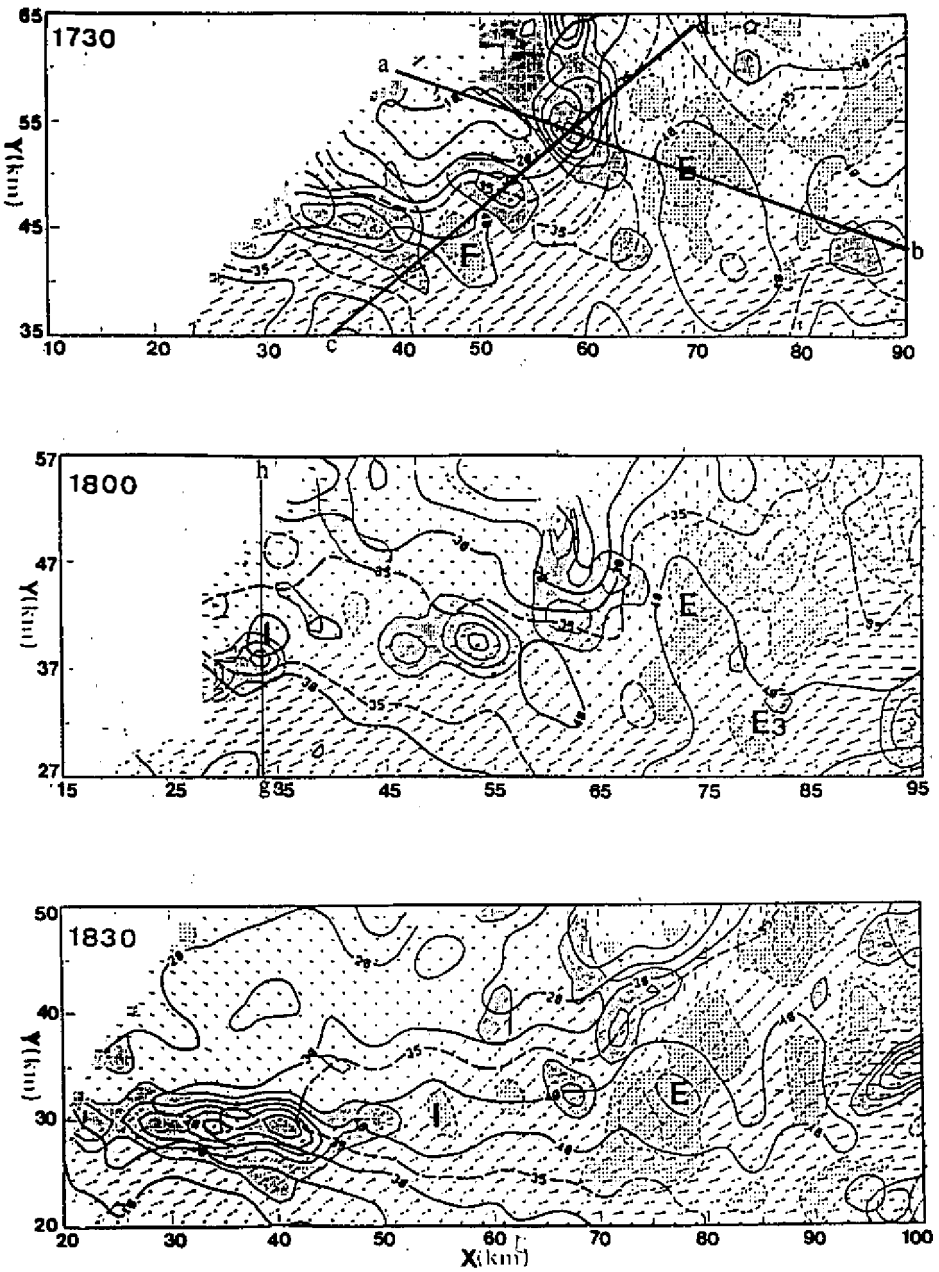

Fig. 4. The horizontal system-relative wind and reflectivity fields at 1 km height for (a) 1730UTC, (b) 1800UTC, and (c) 1830UTC, 24 June. The heavy-shading indicates major convergence area ($<-1.0\times10^{-3}s^{-1}$) and the light-shading indicates major divergence area ($>1.0\times10^{-3}s^{-1}$). E, F, and I are precipitation centers identified in Figure 2.

1830UTC 24 June. The heavy-shading indicates major frontal convergence regions. Accompanying prefrontal intense precipitation centers (E and F in figure 4a and E and I in figure 4c), strong divergences (light-shading) are revealed. The low-level convergence and divergence centers were collocated with mid-tropospheric convective updraft and downdraft centers (figure not shown). The low-level flows showed a pronounced different feature when they approached these precipitation centers. Figures 5 and 6 show the retrieved pressure and temperature perturbations at 1 km height on 1730, 1800 and 1830UTC, 24 June. Negative pressure perturbations correlated well with positive temperature perturbations on the low-level convergent frontal zone. In the prefrontal region, positive pressure perturbations and negative temperature perturbations were present. The prefrontal high pressure, cold temperature air was

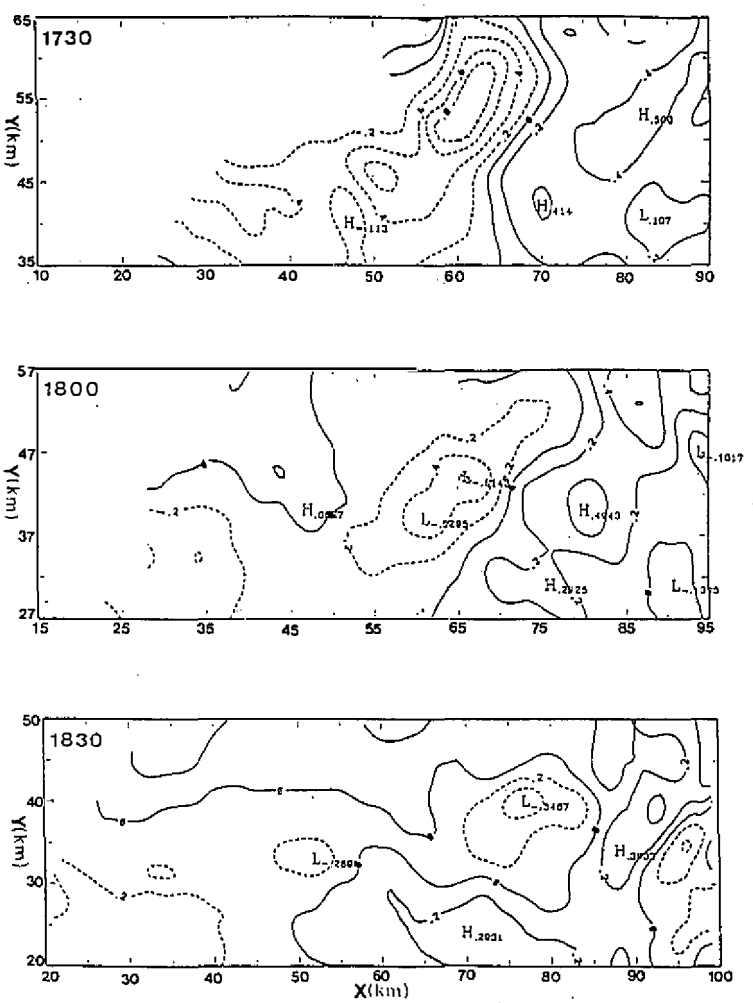

Fig. 5. Same as Figure 4 but for retrieved perturbation pressure in interval of 0.2mb.

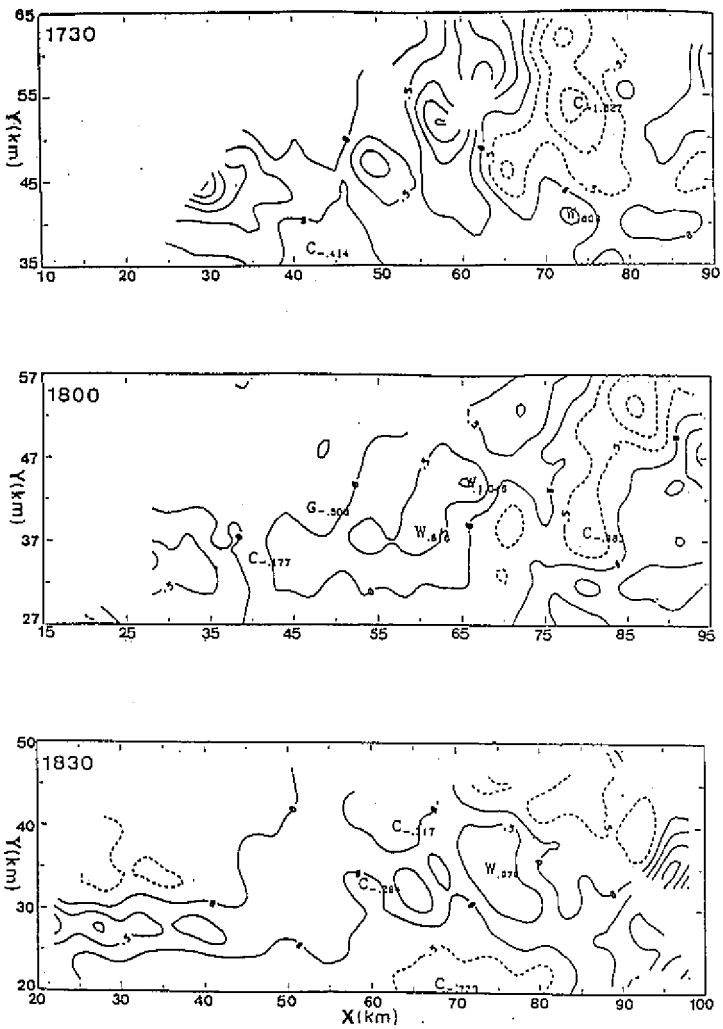

Fig. 6. Same as Figure 4 but for retrieved perturbation temperature in interval of 0.5°C.

limited only in the lower troposphere and correlated well with the major precipitation centers. In the frontal zone, the low pressure, warm temperature air had a much deeper layer and tilted toward the prefrontal region as shown in figure 8 and 9.

It is interesting to note that, the distribution of pressure perturbations at low level shown in Figure 5 suggests that, between the prefrontal mesohigh and the frontal low, a pronounced horizontal pressure gradient presented. It would exert an extra horizontal pressure gradient force on the air parcels travelling along with the prevailing southwesterly LLJ. The consequence of this extra forcing was to deflect the LLJ in the prefrontal region and produce larger horizontal convergence at the frontal zone. This effect was most pronounced when the LLJ

encountered the major precipitation centers in the prefrontal region.

5.2 Evolution of the Convection

In order to have a clearer picture of the evolution of the deep convection embedded within the Mei-yu front, we chose the maximum updrafts and downdrafts within the major convection cells (*i.e.*, cell E, f and I) and plotted them according to sequence of time (see figure 7). It could be seen that F cell was in a state of decaying. It merged with cell E after 1800UTC. In this period, E cell was in a mature state. Cell E reached its maximum intensity at 1730UTC and decayed. After merging with cell F, cell E recovered its original strength and decayed at the end of this period. It was noted that, the intensity of downdraft associated with cell E was rather uniform, about 6-7 ms^{-1}, in this period. How this downdraft was maintained and the effect of this long-enduring storm-scale feature in its immediate environment will be interesting topics for further investigation.

Convective cell I's structures were quite different than E's. Cell I was in a state of developing. Moderate updrafts and no organized downdrafts were observed in the early stage. The updraft reached its maximum intensity at the end of this period. It was noted that no significant convective downdrafts were present until the cell reached its mature development.

Noteworthy in the above discussion, in the same analysis domain, is that different life stages of convective cells were present at the same time. Some were in quasi-steady states in

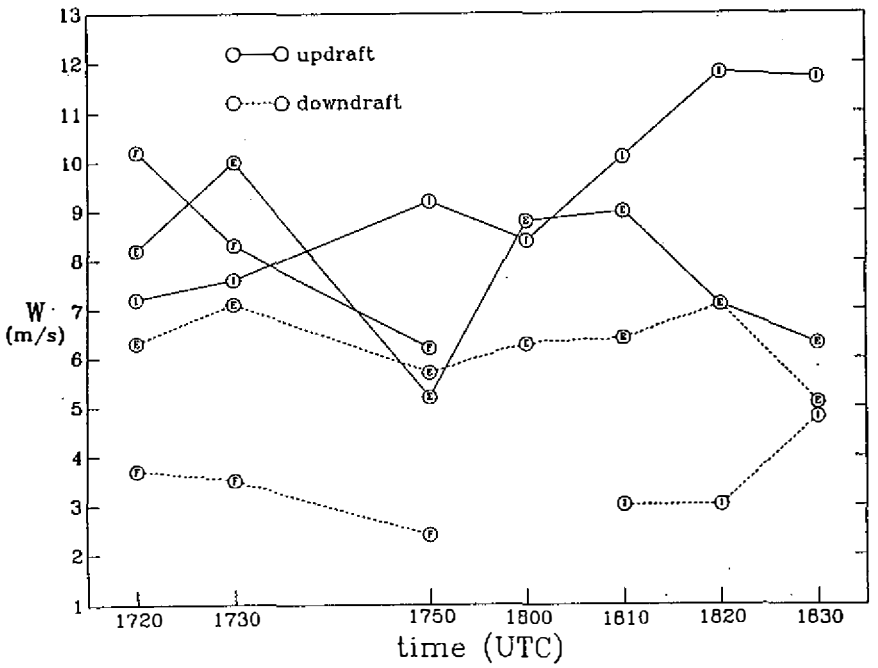

Fig. 7. Time series of the maximum convective updraft and downdraft of precipitation centers shown in Figure 4.

which steady storm-scale updrafts and downdrafts were present. Some were in decaying stage in which the storm-scale updrafts and downdrafts were dissipating. Some were in the developing stage in which the storm-scale updrafts continued to intensify and the organized storm-scale downdrafts appeared. In the next subsection, the structural difference between cells E and I will be discussed.

5.3 Vertical Structure

Figure 8 shows the vertical cross sections of perturbation temperature, perturbation pressure, vertical velocity, reflectivity, and streamlines along line a-b of convective cell E at 1730UTC 24 June. At this time, E cell was in a mature stage. In the frontal zone, there were low pressure, warm anomaly, and convective updrafts. All these features tilted southeastward with height in the direction of shear vector of lower and middle tropospheric environment winds. In the prefrontal region, deep convective downdraft correlated well with deep precipitation centers. Shallow cold air with positive pressure perturbations was found in the prefrontal lower troposphere. The presence of this mesoscale high in the prefrontal region was possibly due to evaporation cooling associated with heavy precipitation.

It was noted the prevailing low-level prefrontal flow was southwesterly and was in a direction perpendicular to cross section a-b (see Figure 4). In order to show the three-dimensional flow structure associated with the convective system, more cross sections are given. In Figure 9, the convection structure along c-d is given. The cross section passes through the updraft center of cell E. The southwesterly flow was deep and reached 4 km height with the maximum wind speed at low-levels. This SW flow collocated with warm temperature and low pressure anomalies. The SW flow was lifted to the upper troposphere in the updraft center. At upper levels (above 9km height), the flow was northeasterly. In cross section c-d, the flow was rather weak in the middle troposphere.

From the above discussion, it can be seen that the flow structure associated with cell E was rather complicated. The inflow of the system was from the southwest. This flow encountered the post-frontal west-northwesterly flow to trigger the convection along the frontal surface. The mid-troposphere northwesterly flow from post-frontal area was the main factor to produce tilted precipitation echoes. This tilted precipitation pattern induced pronounced downward motions in the mid- and lower-troposphere of the prefrontal region. The convective downdrafts and evaporation cooling associated with precipitation provided both dynamic and thermodynamic factors to induce near surface cold pool air and perturbation high pressure features. Although the southwesterly flow had a small angle with the frontal zone, the low-level prefrontal mesoscale high pressure would give the air parcels entering this region an added horizontal acceleration toward the frontal zone. Hence, a stronger horizontal convergence would be established. This structure is important in the sense of scale interaction: the environment-controlled convective-scale features interacted closely with their immediate environmental flow to establish a favorable condition for their own maintenance. This case provides an example how a long-lived convective systems is maintained along Mei-yu front as a result of close interaction between the convective activity and its immediate environmental flow.

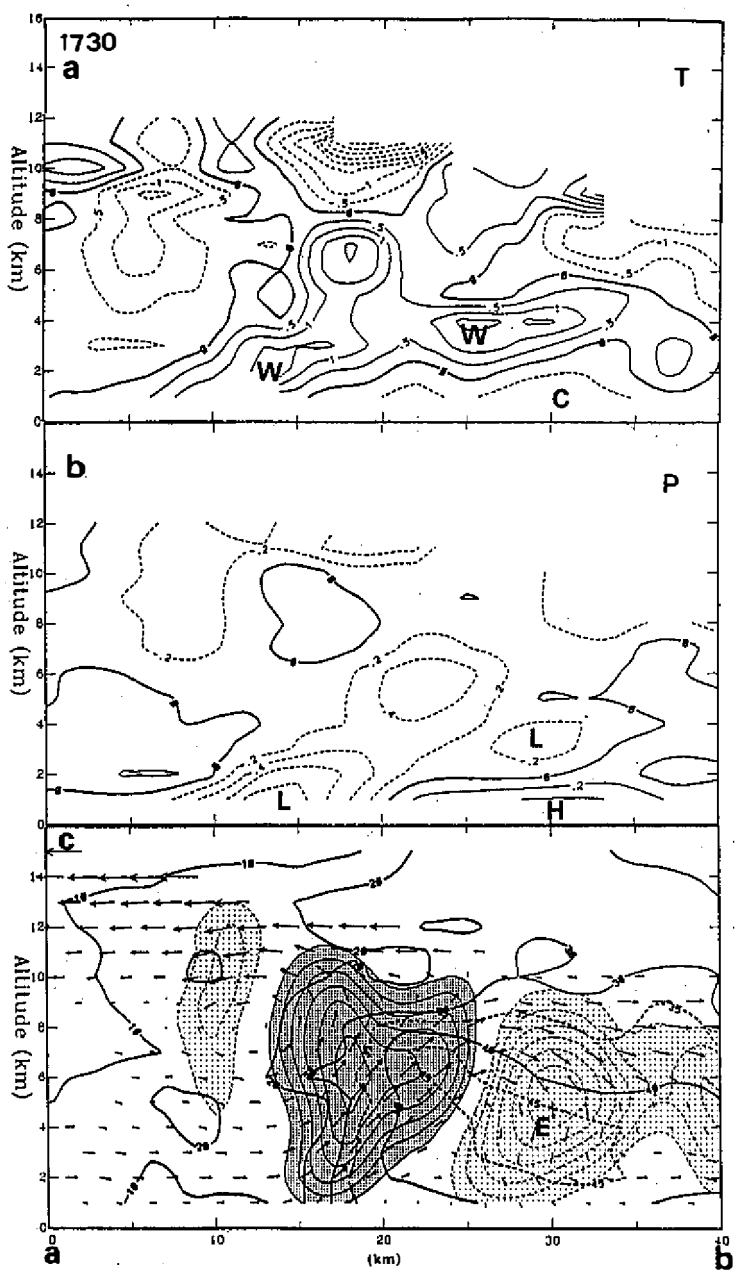

Fig. 8. Vertical cross sections of (a) perturbation temperature (contour interval 0.5°C), (b) perturbation pressure (contour interval 0.2mb), and (c) reflectivity (contour interval 10dBZ) and winds (vertical velocity shaded, heavy-shading for updraft and light-shading for downdraft, contour interval 2ms^{-1}) for cell E along line a-b, 1730UTC 24 June 1987.

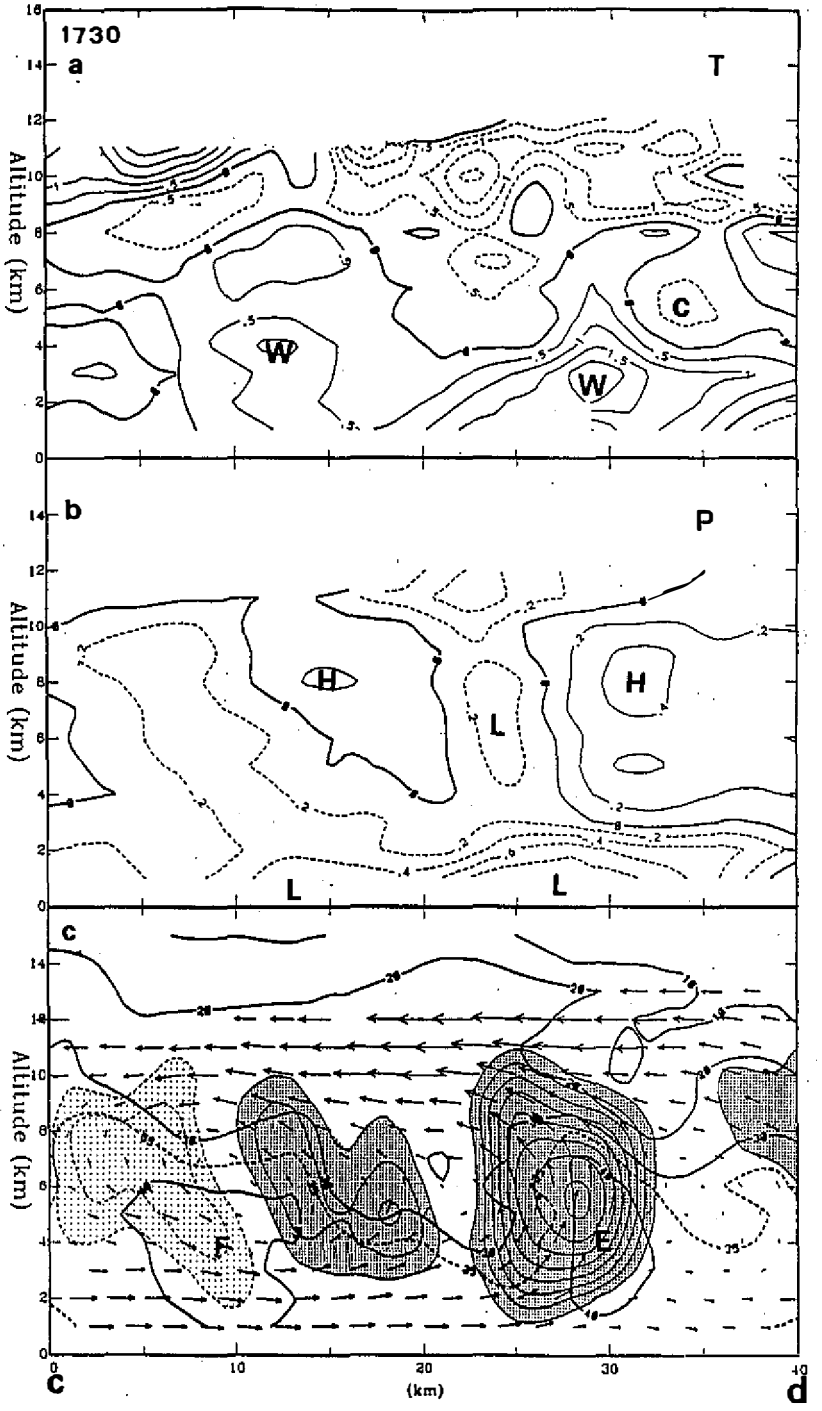

Fig. 9. Same as Figure 8 but for cross sections along line c-d.

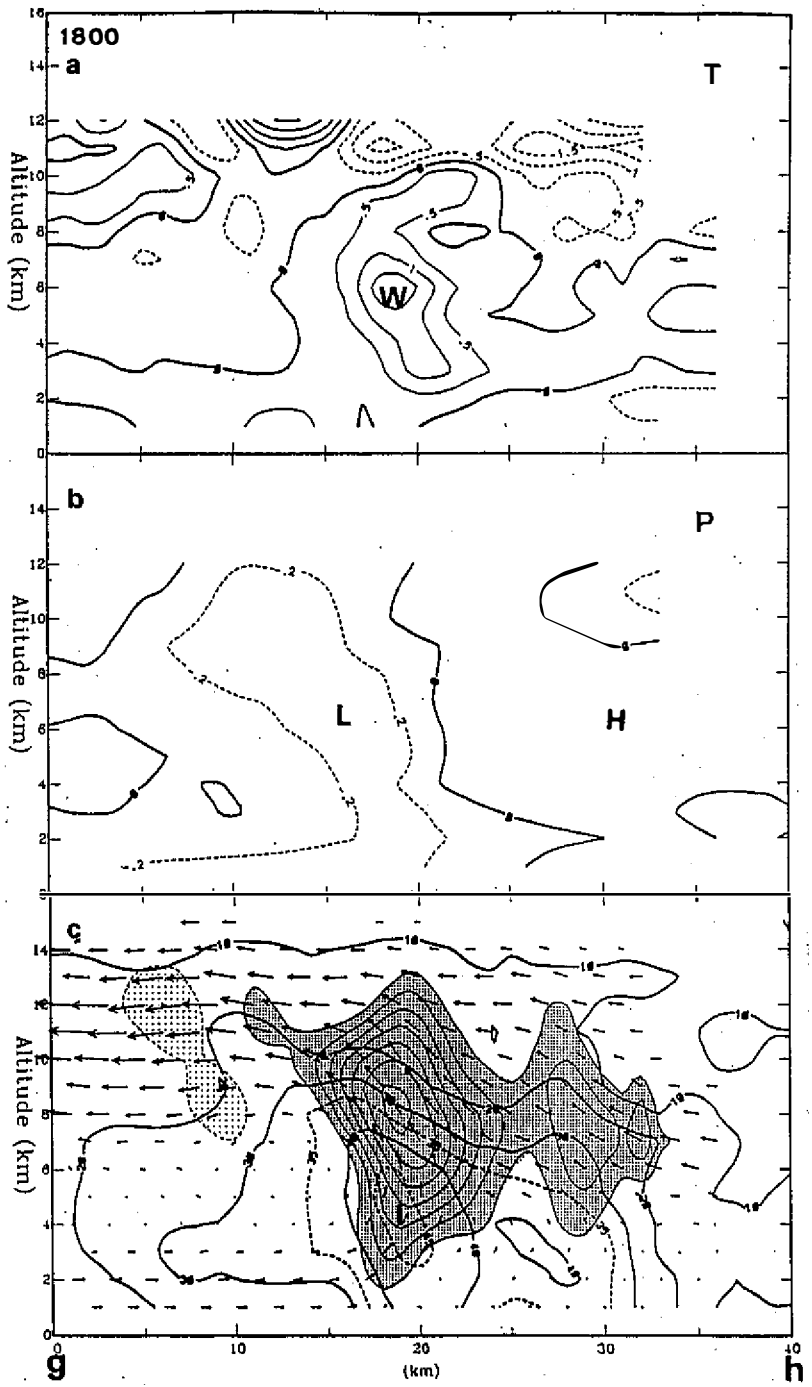

Fig. 10. Same as Figure 8 but for cross sections along line g-h on 1800UTC 24 June.

The structure of cell I at 1800UTC is given in Figure10 which shows the vertical cross sections of all related fields along g-h. Cell I was in a developing stage at this time. The low-level southwesterly flow encountered west-northwesterly flow at the frontal zone. Pronounced horizontal convergence at low levels existed (see Figure 4). The organized convective upward motions were found at the warm-side of frontal zone and collocated with major precipitation center. This storm-scale feature is quite different from what was observed in cell E in which the major precipitation center was tilted to the prefrontal region and collocated with convective downward motions. Cell I did not present major convective downward motions at this time and, consequently, no low-level cold air or mesoscale high pressure system was found. This observation, combined with what was discussed above, suggests that the formation of organized convective downdrafts in a convective storm play a major role in interacting with its immediate environment. This interaction is important in the sense that such a change of the environment would produce a favorable environmental condition for convection to grow. The observation also suggests that, in the Mei-yu front, the formation of organized convective downdraft is a sign for the possible occurrence of a long-lived convective system.

6. CONCLUDING REMARKS

A convective frontal rainband observed by TAMEX Doppler network was investigated in this paper. The results show that there were at least two types of organization of convection in the Mei-yu front. Type A is the shallow convection triggered by colliding cold air surface with the prevailing southwesterly flow. This type of convection was observed on the cold-air leading edge of the surface cold front. The convection is shallow and has the maximum vertical motions at low levels. The occurrence of maximum rainfall follows the passage of surface cold front and dissipates rapidly. The appearance of strong vertical wind shear along the interface of the surface cold air and the lifted prevailing southwesterly flow provide the possibility of forming wave-type disturbances in the post-frontal region through Kelvin-Helmholtz instability. These wave-type disturbances would modulate convection activity in the post-frontal region. This mechanism resembles a feature very similar to features frequently observed in mid-latitudes in colliding gust fronts associated with thunderstorm outflows.

Type B is the long-lived deep convection systems that occur in the prefrontal region. This type of convection possessed complicated three-dimensional convective-scale features and is produced by a close interaction between the convective-scale features and their immediate mesoscale environmental flows. The tilted convective updrafts, the intense convective downdrafts, the formation of prefrontal mesoscale high pressure system, the deflected low-level jet between the frontal zone and the prefrontal mesohigh, and the distorted frontal surface as revealed in vertical component of relative vorticity field, all play important roles in formation, organization, and maintenance of these convective systems. This paper only presents a preliminary investigation of this topic. Further studies are needed in order to explore more detailed structural and dynamic aspects of these heavy-rainfall producers in the Taiwan Mei-yu season.

Acknowledgements Support for this research was provided by National Science Council of Republic of China under grants NSC86-2111-M002-005-Ap6.

REFERENCES

Carbone, R. E., 1982: A severe frontal rainband. Part I: Storm wide hydrodynamic structure. *J. Atmos. Sci.*, **39**, 258-279.

Chi, S.-S., and G. T.-J. Chen, 1989: A study on the MCS case of TAMEX IOP-13. Proc. Workshop on TAMEX Preliminary Scien. Results, June 20-30, Taipei, Taiwan, 14-21.

Hobbs, P. V., 1978: Organization and structure of clouds and precipitation on the mesoscale and microscale in cyclonic storms. *Rev. Geophys. Space Phys.*, **16**, 741-755.

Hobbs, P. V., and K. R. Biswas, 1979: The cellular structure of narrow cold frontal rainband. Quart. *J. Roy. Meteor. Soc.*, **105**,723-727.

Hobbs, P. V., and P. O. G. Persson, 1982: The mesoscale and microscale structure and organization of clouds and precipitation in midlatitude cyclones. Part V: The substructure of narrow cold-frontal rainbands. *J. Atmos. Sci.*, **39**, 280-295.

James, P. K., and K. A. Browning, 1979: Mesoscale structure of line convection at surface cold fronts. Quart. *J. Roy. Meteor. Soc.*, **105**, 371-382.

Jou, B. J.-D., and S.-M. Deng, 1992: Structure of a low-level jet and its role in triggering and organizing moist convection over Taiwan: a TEMAX case study. *TAO*, **3**, 39-58.

Kuo, Y. H., and G. T.-J. Chen, 1990: Taiwan Area Mesoscale Experiment: An overview. *Bull Amer. Meteor. Soc.*, **71**, 488-503.

Li, J., Y.-L. Chen, and W.-C. Lee, 1997: Analysis of a heavy rainfall event during TAMEX. *Mon. Wea. Rev.*, **125**, 1060-1082.

Lin, P.-L., T.-C. C. Wang, and C.-C. Yeh, 1989: Doppler observational study of a long-lived rainband in TAMEX IOP-13. *Paper Meteor. Res.*, **12**, 91-120.

Lin, Y.-J., R. W. Pasken, and H.-W. Chang, 1992: The structure of a subtropical prefrontal convective rainband. Part I: Mesoscale kinematic structure determined from dual-Doppler measurements. *Mon. Wea. Rev.*, **120**, 1816-1836.

Lin, Y.-J., H.-W. Chang, and R. W. Pasken, 1993: The structure of a subtropical prefrontal convective rainband. Part II: Thermodynamic and dynamic structure and momentum budget. *Mon. Wea. Rev.*, **121**, 1223-1254.

Mannouji, N., and K. Kurihara, 1990: A numerical experiment of TAMEX IOP 13 by the spectral limited area model of the JMA. Proc. Workshop on TAMEX Scien. Results, Sept. 24-26, Boulder, CO., 121-126.

Mueller, C. K., and R. E. Carbone, 1987: Dynamics of a thunderstorm outflow. *J. Atmos. Sci.*, **44**, 1879-1898.

Orlanski, I., and B. B. Ross, 1984: The evolution of an observed cold front. Part II: Mesoscale dynamics. *J. Atmos. Sci.*, **41**, 1669-1703.

Ross, B. B., and I. Orlanski, 1982: The evolution of an observed cold front. Part I: Numerical simulation. *J. Atmos. Sci.*, **39**, 296-327.

Simpson, J. E., 1969: A comparison between laboratory and atmospheric density currents. *Q. J. Roy. Meteor. Soc.*, **95**, 758-765.

Trier, S. B., D. B. Parsons, and T. J. Matejka, 1990: Observations of a subtropical cold front in a region of complex terrain. *Mon. Wea. Rev.*, **118**, 2449-2470.

Wakimoto, R. M., 1982: The life cycle of thunderstorm gust fronts as viewed with Doppler radar and rawinsonde data. *Mon. Wea. Rev.*, **110**, 1113-1140.

Weckwerth, T. M., and R. M. Wakimoto, 1992: The initiation and organization of convective cells atop a cold-air outflow boundary. *Mon. Wea. Rev.*, **120**, 2169-2187.